Resonant peak in the output spectral profile of an ionic anti-Stokes Raman laser

S. A. Babin, S. I. Kablukov, S. V. Khorev, E. V. Podivilov, V. V. Potapov, D. A. Shapiro, and M. G. Stepanov
Institute of Automation and Electrometry, Siberian Branch, Russian Academy of Sciences, Novosibirsk 630090, Russia
(Received 5 May 2000; revised manuscript received 13 November 2000; published 8 May 2001)

Continuous-wave generation of the anti-Stokes Raman laser is demonstrated in the new Λ scheme Ar II $3d'\,^2G_{9/2}\rightarrow 4p'\,^2F_{7/2}\rightarrow 4s'\,^2D_{5/2}$ with quasimetastable initial and final levels. Red pump radiation with wavelength $\lambda_p=611$ nm from a dye laser that excites transition $3d'\,^2G_{9/2}\rightarrow 4p'\,^2F_{7/2}$ is converted into the blue radiation at $\lambda=461$ nm ($4p'\,^2F_{7/2}\rightarrow 4s'\,^2D_{5/2}$) with efficiency of about 30%. The tunability range spans more than 20 GHz around exact resonance, which is five times broader than the Doppler contour. The output frequency ω is found to depend linearly on the frequency ω_p of the pump field: $\omega\simeq\omega_p\lambda_p/\lambda$. A sharp peak of output power is observed in the spectral profile at the exact resonance instead of the well-known two-photon dip. The model is proposed that includes ionic scattering in plasma and interaction of the running pump and standing output waves. The theory offers an interpretation of the observed peak.

DOI: 10.1103/PhysRevA.63.063804 PACS number(s): 42.55.Ye, 32.70.Jz, 52.20.Hv

I. INTRODUCTION

Many interesting optical effects have attracted particular interest in Raman lasing. Recent examples are nonlinear dynamics, including longitudinal-mode competition and bistability [1], inversionless gain [2], amplification of ultrashort pulses [3], suppression of quantum noise [4], intracavity electromagnetically induced transparency [5], and creation of the population inversion on transitions involving the ground state [6]. Meanwhile, one of major purposes of these efforts is to achieve the short-wavelength amplification and generation (for reference list see [7–9]).

Up-conversion methods are based in general on 3- and 4-level systems. Most progress has been made toward that goal in four-wave mixing schemes [10–12]. However, in the mixing experiments the efficiency was low [10], or the frequency shift was small [11], or the output radiation was not continuous [12]. Proposed ''inversionless'' gain schemes with large shifts [13] have not been experimentally confirmed yet. Thus, in spite of obvious achievements, in principle demonstrations, realization of the continuous powerful up conversion with large frequency shift remains an unsolved problem.

In this view, the Raman Λ scheme, Fig. 1, is still of interest, especially its capability of short-wave generation. The largest frequency shift in continuous mode, from the red to blue spectrum, has been obtained in argon plasma [14,15]. In the experimental configurations, $3d$-metastable levels were used as the starting ones (n), while short-lived $4s\,^2P_{1/2,3/2}$ served as the final levels (l). This group of states is thoroughly studied, since they are utilized as lower levels in argon-ion laser transitions. The chosen combination of lifetimes provides the maximum population inversion on the Raman transition nl, and as a result, the conversion efficiency increase up to 60%. Since the main lasing channel is provided by the stepwise process, the tunability range for that scheme is limited by the Doppler width. Pump photon is absorbed on the transition nm from initial to intermediate state m, after that the output photon is emitted on the adjacent transition ml.

Schemes with long-lived final level realized in atomic gases, e.g., Ne I [16], have lower conversion coefficient (less than 10%), whenever their tunability range exceeds 100 Doppler widths. The physical reason is the two-photon process that is predominant in these schemes. Simultaneous absorption of the pump photon and emission of the output photon occur. A narrow dip has been predicted in the output spectrum having the width of forbidden transition (see, e.g., Refs. [17,18]). This two-photon dip was observed in the neon Λ scheme $2p_1\rightarrow 2s_2\rightarrow 2p_4$ with wavelengths $\lambda_p=1.5$ and $\lambda=1.15$ μm [19]. The spectral profile displayed a dip with the width of forbidden transition between the initial and the final levels.

In the present paper, the scheme of up conversion is proposed for Ar II transitions $3d'\,^2G_{9/2}\rightarrow 4p'\,^2F_{7/2}\rightarrow 4s'\,^2D_{5/2}$ with a relatively long-lived final state. Level lifetimes in this scheme are close to that in Ne I, while the wavelength shift is much greater. In spite of the close parameters, our measurement does not reveal the expected two-photon dip. A sharp peak is observed in the center of the spectral profile instead.

In contrast to other gas lasers, an additional broadening of nonlinear resonances occurs in ion lasers, in particular the two-photon resonance gets broadened. Analysis of the Coulomb broadening due to ion scattering in plasma is based on a Fokker-Plank type kinetic equation (see Refs. [20] and references therein). The small-angle scattering leads to diffusion in the velocity space. This theory was limited by the domain of weak saturation, whereas the strong-field effects

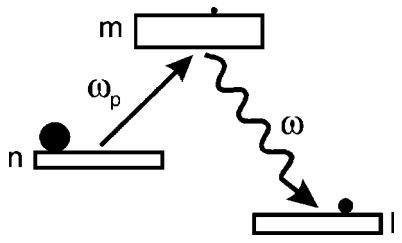

FIG. 1. Raman Λ configuration with Bohr frequencies $\omega_{mn}=(E_m-E_n)/\hbar$ and $\omega_{ml}=(E_m-E_l)/\hbar$, E_j are the levels of energy. The widths of levels are shown schematically by the boxes. Circles denote relative populations.

are important to explain the intracavity photon-ion interaction in the Raman laser.

Now the theory is expanded to the case of a strong field in a standing-wave mode. It occurs that either two-photon, or other optical coherence effects are suppressed by the diffusion of phase and turn out to be negligible under a strong field. The only essential broadening is that of population distribution over velocity. The derived expression is appropriate to interpret the peak in the spectral profile, i.e., the output power as a function of the pump frequency.

In Sec. II, we describe the experimental setup. The frequency curve, i.e., the dependence of output frequency on the input one, is shown to be a linear function. The spectral profile with the sharp peak in the center is presented.

In Sec. III, the equations for the density matrix are solved for a three-level Λ system with Coulomb scattering. Section III A introduces the kinetic equation for ionic Λ scheme, where we take into account the Coulomb small-angle scattering but ignore the contribution of higher spatial harmonics of standing wave (rate equations) and the coherence effects. Section III B contains estimations of experimental plasma parameters. It is shown that under the considered conditions the diffusion of phase has managed to destroy the coherence between initial and final states. Thus we can ignore the two-photon process with respect to optical pumping. In Sec. III C, the Raman amplification, i.e., the power of standing wave generated in unit volume, is calculated. The simple formula obtained corresponds to a quantum amplifier with optically short active medium neglecting spontaneous decay. In Sec. III D, the more realistic problem is treated. We take into account the propagation effects, i.e., solve the kinetic equation for ions together with equations for the field. The spontaneous decay is also accounted. The formula for self-consistent output power as a function of input detuning is derived.

Section IV is devoted to comparison between the theory and experiment. The least-square fitting with reasonable parameters is performed. Validity domains of the theoretical model are discussed. Section V summarizes the results.

II. DETUNING CHARACTERISTICS

The three-level Λ scheme is shown in Fig. 1. The input pumping field resonant to transition mn with frequency ω_p is converted into output field with frequency ω, resonant to transition ml. The wavelengths for Ar II $\lambda_p = 611$ nm and $\lambda = 461$ nm correspond to up-conversion. Starting level n ($3d'^2G_{9/2}$) is metastable, its radiative decay into the ground state $3p^5\,^2P_{3/2}$ is forbidden by the $\Delta J = 0,1$ selection rule. However, in gas-discharge plasma the lifetime of level n is limited by inelastic collisions with electrons and amounts to $\Gamma_n^{-1} \approx 40$ ns [15,21]. For final level l ($4s'^2D_{5/2}$) the dipole transition into ground state is also forbidden, since the parent Ar III configuration changes. Nevertheless, this rule is not strict for Ar II, hence the characteristic radiative lifetime is in the interval $\Gamma_l^{-1} \approx 10$–27 ns according to calculations by different authors [22,23]. The intermediate level m ($4p'^2F_{7/2}$) is similar to the laser level $4p'^2F_{5/2}$. The latter is used as the upper level of laser line 501.7 nm, and is well studied. Its radiative lifetime is 8.5 ns. The electron deactivation decreases this value to $\Gamma_m^{-1} \approx 6$ ns, see Ref. [20]. Thus, the inequality $\Gamma_n, \Gamma_l \ll \Gamma_m$ is roughly valid.

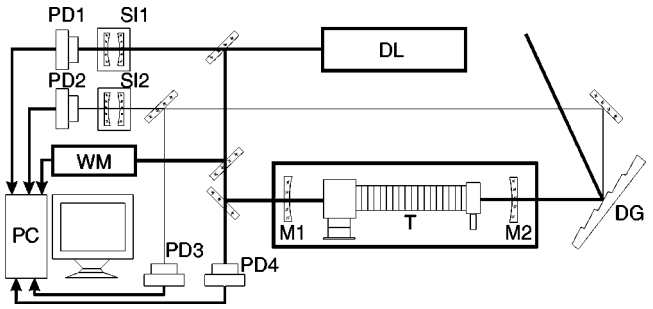

FIG. 2. Experimental setup: DL, dye laser; T, discharge tube; M1, M2, mirrors of the Raman laser cavity; DG, diffraction grating; SI1 and SI2, scanning interferometers; PD1, PD2, PD3, and PD4, photodetectors; WM, wavelength meter, PC, computer.

The off-diagonal relaxation constant Γ_{nl} of forbidden transition is much less than those of allowed transitions Γ_{mn}, Γ_{ml}. In this case, the effects of two-photon coherence should prevail in the three-level system considered. The ratio of relaxation constants and their absolute values are close to that of the Raman laser in atomic neon $2p_1 \rightarrow 2s_2 \rightarrow 2p_4$. In neon, the coherence effects led to a narrow dip that appeared in the center of the spectral profile. The width of the dip is given by the constant Γ_{nl} of the forbidden transition.

Level populations in the argon-laser plasma are governed by the balance between radiation and the collision processes. In the scheme under consideration they are $N_n \approx 10^{11}$ cm$^{-3} \gg N_l \sim N_m \approx 10^{10}$ cm^{-3} [21]. The starting level is much more populated than other levels. Population inversion on transition ml in conventional discharge is absent, correspondingly the continuous generation was never observed at this line, see Refs. [24,25].

A sketch of the experimental setup is shown in Fig. 2. Active medium of the Raman laser was created by means of the low-pressure discharge at current $I \approx 100$ A in 7-mm-bored tube T. The length of active part was $L = 50$ cm. Homogeneous pressure distribution along the tube axis was kept with the help of a slow longitudinal flow of gas [26]. The continuous-wave dye laser (DL) with Rh6G was used for pumping. Its power was up to 100 mW in single-frequency mode at the wavelength of 611 nm. The pump radiation was directed by mirrors into the tube T. Internal mirrors M1, M2 were attached to tube ends by means of vacuum bellows. The reflection coefficient of the mirrors was high at 461 nm and low at 611 nm. The output transmission at 461 nm in the first experiment was about $T \simeq 0.3\%$. An absorption of the weak signal was also measured; in this measurement the power of the dye laser was lowered. The red and blue lines were separated with diffraction grating (DG). The spectra of the dye and Raman lasers were registered by scanning interferometers SI1, SI2, photodiodes PD1, PD2 and λ-meter WM ''Angstroem'' with a sensitivity of 8 digits (down to 10 MHz in frequency units). The power was measured with photodiodes PD3 and PD4.

During the scanning of pump frequency the data were synchronously written by a PC. Recorded data gave two ex-

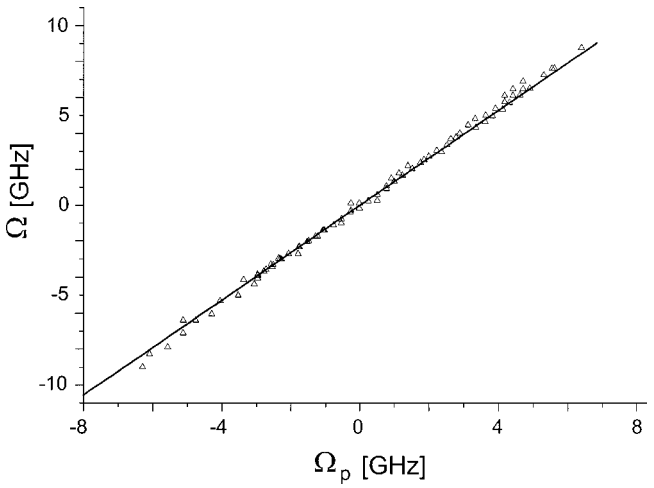

FIG. 3. Frequency correlation: the measured dependence of generated frequency detuning $\Omega=\omega-\omega_{ml}$ on the detuning of pumping frequency $\Omega_p=\omega_p-\omega_{mn}$. The solid curve is a straight line with slope k/k_p.

perimental curves: the generated frequency ω as a function of pump frequency ω_p (Fig. 3) and the output power W_{AS} as a function of pump frequency ω_p (Fig. 4).

Analyzing the data of frequency measurement we conclude that the generation frequency is proportional to the pumping one:

$$\frac{\Omega}{k}=\frac{\Omega_p}{k_p}. \tag{2.1}$$

Here $\Omega=\omega-\omega_{ml}$ and $\Omega_p=\omega_p-\omega_{mn}$ are the detunings. A typical series of experimental points in Fig. 3 proves dependence (2.1). At different parameters, no deviation from the linear law was observed and the slope was constant. Some scattering of points is originated from jumps between longitudinal modes of the cavity (about 100 MHz). The detuning range of the Raman laser exceeded 5 Doppler widths ($kv_T=3.2$ GHz). The conversion efficiency at the center was as high as 30%.

The most unexpected feature was observed in the spectral profile, Fig. 4. It was a sharp peak at the center instead of the dip typical for neon atomic lines [19]. The characteristic width of the peak, 500–800 MHz, was much greater than the expected width $\Gamma_{nl}\approx 20$ MHz of forbidden transition. The curve had a three-scale structure: a relatively narrow peak at the center, the smooth dip of the nearly Doppler width around, and wide wings. The wings (and consequently, the tunability range of the Raman laser) were almost independent of the discharge parameters and pump power. The dip exhibited more sensitivity to the discharge current and pressure and disappeared at low currents $I\leqslant 40$ A. It became deeper, on the other hand, by decreasing the pump power. At low-intensity pumping, the generation at the center vanished and a gap formed in the spectral profile with the width about kv_T. Here, the generation remained outside the Doppler width.

Surprisingly, in the ''high-Q'' cavity ($T=0.3\%$) the generation on the ml transition (461 nm) appeared under lower argon pressure $p<0.1$ torr even without pumping. Note that the continuous laser oscillation at this line was never observed, while pulsed generation has been obtained under specific conditions [24]. In our device, long-term operation under low pressure was hard because of discharge instabilities that shorten the tube lifetime. Although experiment in this regime was difficult, it was helpful, since it allowed us to find the reason of the dip formation and to provide the Raman lasing in a ''low-Q'' cavity ($T=7\%$).

It was clarified that the dip in the spectral profile was caused by nonuniform pressure distribution along the discharge axis [26]. Cathode and anode bulbs contained colder ions under higher pressure compared to the plasma column. Under condition $N_m\approx N_l$, the contribution of the electrode layers into absorption leads to significant perturbation of the

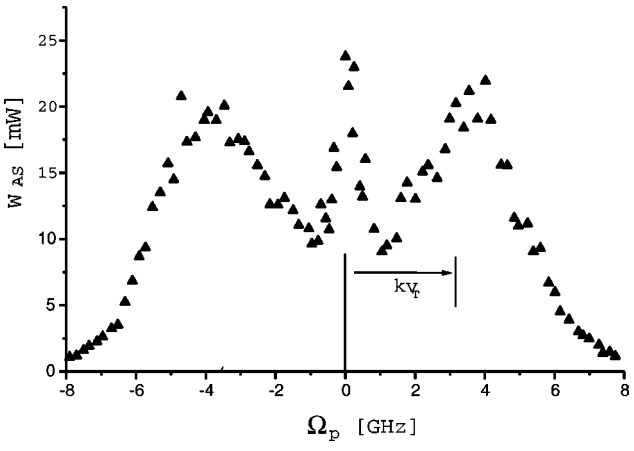

FIG. 4. Spectral profile in the ''high-Q'' cavity ($T=0.3\%$): the generated power W_{AS} as a function of the pump frequency detuning Ω_p at current 100 A, pressure 0.2 Torr. For comparison, the Doppler width kv_T is shown in the graph. The sharp peak at the center is discussed in Sec. IV.

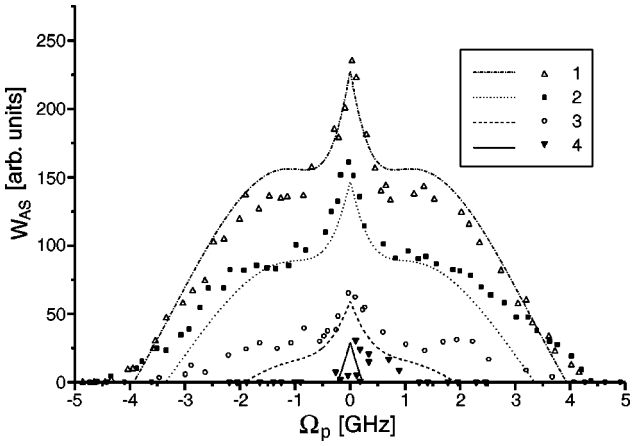

FIG. 5. Measured spectral profiles in ''low-Q'' cavity ($T=7\%$) at current 70 A along with theoretical curves: $P/\tau=6.89$ (80 mW), $\mathcal{N}/\tau=0.53$ (curve 1); $P/\tau=4.65$ (54 mW), $\mathcal{N}/\tau=0.53$ (curve 2); $P/\tau=2.33$ (27 mW), $\mathcal{N}/\tau=0.53$ (curve 3); $P/\tau=2.33$ (27 mW), $\mathcal{N}/\tau=0.0056$ (curve 4). Pressure was 0.1 Torr (curves 1,2, and 3) or 0.15 Torr (curve 4).

Doppler line for ml transition. In particular, there existed an operation mode with the absorption at the line center and amplification at wings. The effect manifested itself in multimode generation (without pumping); its spectral profile, measured near the threshold at high pressure, showed a wide dip that disappeared at lower pressure. It means that similar effect should exist in the spectral profile of small signal gain.

Under lower pressure, when the longitudinal distribution was more smooth, the Raman lasing could be observed in the transparent cavity, i.e., at $T=7\%$. When the pump was off, the integral gain was less than the losses for output mirror transmission. The power of dye laser of about 10 mW (intensity 0.4 W/cm^2) was enough for lasing. Experimental curves, recorded at different discharge parameters and pump power showed no dip, Fig. 5. A sharp peak was evident against the background of the broad wings. The relative peak height was within 30–50 % in the wide domain of parameters. At low pumping power and relatively high pressure, a single isolated peak was observed without wings. However, the accuracy of measurement under these conditions was low due to strong fluctuations near the threshold. A model interpreting the peak is discussed in the next section.

III. COULOMB DIFFUSION UNDER A STRONG FIELD

A. Basic equations

The standing output wave has the form

$$\mathcal{E}(x,t)=\mathcal{E}\,e^{-i\omega t}(e^{ikx}+e^{-ikx})+\text{c.c.},$$

where frequency ω is close to Bohr frequency of transition ml, x is the coordinate along the cavity, and c.c. means the complex conjugate term. Let us write the off-diagonal element of the density matrix ignoring higher spatial harmonics $e^{3ikx}, e^{5ikx}, \ldots$:

$$\rho_{ml}(x,u,t)=e^{-i\omega t}[e^{ikx}\rho_+(u)+e^{-ikx}\rho_-(u)].$$

Polarizations ρ_+ and ρ_- are induced by the waves running in positive and negative directions, respectively. Here u is the projection of the velocity **v** onto the wave vector **k**. The power of induced emission is given by the integral over velocities

$$\mathcal{P}(\Omega)=2\hbar\omega\ \mathrm{Re}\int du[iG^*(\rho_+(u)+\rho_-(u))], \quad (3.1)$$

where $G=\mathcal{E}\mu_{ml}/2\hbar$ is the Rabi frequency of the probe field, and μ_{ml} is the dipole moment of transition ml.

In experiment, the external pumping field on transition mn enters the cavity

$$\mathcal{E}_p(x,t)=\mathcal{E}_p e^{i(k_p x-\omega_p t)}+\text{c.c.}$$

That is a traveling wave propagated in a positive direction. It excites ions from the long-lived level n to the upper level m, increasing, in doing so, the population inversion on the working transition ml.

Amplitudes $\rho_\pm(u)$ could be found from the kinetic equation [20]

$$[\Gamma_{lm}-i(\Omega\mp ku)]\rho_\pm=\hat{\mathcal{V}}\rho_{lm}-iG(\rho_m-\rho_l),$$

$$\Gamma_l\rho_l=\hat{\mathcal{V}}\rho_l+2\ \mathrm{Re}[iG^*(\rho_++\rho_-)]+A_{ml}(\rho_m-\rho_m^0)+\Gamma_l\rho_l^0,$$

$$\Gamma_m\rho_m=\hat{\mathcal{V}}\rho_m-2\ \mathrm{Re}[iG^*(\rho_++\rho_-)]-2\ \mathrm{Re}(iG_p^*\rho)+\Gamma_m\rho_m^0, \quad (3.2)$$

$$[\Gamma_{mn}-i(\Omega_p-k_pu)]\rho=\hat{\mathcal{V}}\rho-iG_p(\rho_m-\rho_n),$$

where $\rho_j\equiv\rho_{jj}$ is the population of level j, $\rho(u)=\exp[-i(k_px-\omega_pt)]\rho_{mn}$ is the polarization induced by the pumping field, Γ_j and Γ_{ij} are the relaxation constants for level j and polarization ρ_{ij}, $\Omega=\omega-\omega_{ml}$ and $\Omega_p=\omega_p-\omega_{mn}$ are the same detunings of the output and pump waves with respect to the corresponding Bohr transition frequencies, as in Eq. (2.1), A_{ml} is the Einstein coefficient, $G_p=\mathcal{E}_p\mu_{mn}/2\hbar$ is the Rabi frequency for pump wave, μ_{mn} is the dipole moment of transition mn, $\rho_j^0=N_j\exp(-u^2/v_T^2)/\sqrt{\pi}v_T$ is the equilibrium population of level j without the field, which has a shape of one-dimensional Maxwellian distribution with thermal velocity $v_T=\sqrt{2T_i/m}$, where T_i is the ion temperature in the energy units, and m is the ion mass. In the equation for the density matrix we drop out the terms proportional to polarization ρ_{nl} at the forbidden transition and contribution of the higher spatial harmonics.

The operator of small-angle ion-ion scattering $\hat{\mathcal{V}}$ describes the velocity change of an ion. Random wandering of the ion in the microfield of other charged particles can be presented as a diffusion in velocity space:

$$\hat{\mathcal{V}}=D\frac{d^2}{du^2},\quad D=\frac{8\sqrt{\pi}Ne^4}{3m^2v_T}\Lambda,$$

where D is the diffusion coefficient, N,e are the ion density and charge, and Λ is the Coulomb logarithm [27].

B. Approximation of strong Coulomb diffusion

The pumping field is in resonance with ions having velocity $u_*=\Omega_p/k_p$. Nonlinear correction to the population distribution (the Bennett holes) reaches maximum at $u=u_*$. In a similar way, the generated field is in resonance with ions of velocity $u_*=\pm\Omega/k$ for the wave running in the positive $(+)$ or negative $(-)$ direction, respectively. Nonlinear corrections $\delta\rho_j(u)=\rho_j-\rho_j^0$ that appear because of interaction with the fields, have the shape of narrow peaks or dips with extrema at resonant velocities u_*. Since the random velocity change of an ion in plasma follows the diffusion law $\sqrt{Dt}$, the width of a nonlinear structure cannot be less than the diffusion width $\Delta u=\sqrt{D/\Gamma_j}$. Under typical experimental conditions $\Gamma_j\sim2\times10^8\ \mathrm{s}^{-1}$, $kv_T\sim2\times10^{10}\ \mathrm{s}^{-1}$, $Dk^2\sim(2\times10^9\ \mathrm{s}^{-1})^3$, $N\sim10^{14}\ \mathrm{cm}^{-3}$, and $T_i\sim1$ eV, we can take advantage of the following inequalities:

$$\frac{\Gamma_{lm}}{k},\frac{\Gamma_{mn}}{k_p}\ll\sqrt{\frac{D}{\Gamma_j}}\ll v_T.$$

From the first relation it follows that the diffusion width Δu of the corrections is much greater than their collisionless widths. The second relation means that the diffusion width is small compared to thermal velocity v_T.

If we neglect ion-ion collisions, the gain for the generated wave is induced by optical pumping processes, caused by population transfer from level n to m, and coherent two-photon processes, caused by polarization ρ_{nl} on the forbidden transition. In our case the contribution of two-photon processes can be ignored, since the polarization ρ_{nl} is suppressed by the Coulomb diffusion. Pump and probe waves do modulate the polarization as $\exp[i(k-k_p)x]$, then ρ_{nl} turns to zero if the statistical uncertainty of particle coordinate Δx approaches $\pi/(k-k_p)$. Value Δx is defined by the velocity diffusion $\Delta x=\Delta u\, t$ and grows up with time as $\Delta x \simeq D^{1/2}t^{3/2}$. Hence the time of dephasing can be estimated as $\tau_D \simeq [D(k-k_p)^2]^{-1/3} \sim 10^{-9}$ s. That is much less than the relaxation time Γ_{nl}^{-1} at the forbidden transition. This relation among times signifies the strong damping of polarization and the possibility of neglecting two-photon coherent processes in the kinetic equation (3.2).

Thus, the gain of the generated standing wave has two peaks at resonant frequencies $\Omega=\pm\Omega_p k/k_p$. Their heights are nearly equal; the width of each is controlled by the diffusion $\Delta\Omega=k\sqrt{D/\Gamma_m}$. The small-signal gain is independent of the sign of detuning, therefore, both waves seemingly must come to generation. However, even a tiny contribution of coherence effect to the gain coefficient of one wave breaks the symmetry and gives an advantage to one of the two possibilities. This disbalance is enhanced by the nonlinear mode competition [28], as a result the generation occurs only at $\Omega=+\Omega_p k/k_p$. At the same time, the influence of coherence processes on the generation power is negligible provided $|\Omega_p|<k_p v_T$.

The formation of a single peak in the center of the spectral profile [Figs. 4 and 5] can be explained merely by population effects. Let us consider the distribution of polarization over velocity u. The population difference $\Delta N_{ml}(u)=\rho_m(u)-\rho_l(u)$ at the maximum of nonlinear correction $\delta\rho_m$, $u=u_*=\Omega_p/k_p$, within the Doppler contour is almost independent of Ω_p. Then, the gain for the copropagating wave is independent of the detuning, too.

At small detuning $\Omega_p \lesssim k_p\sqrt{D/\Gamma_m}$, the wave running in the negative direction may also be amplified due to the population inversion created by the pumping field. Conversely, when the detuning exceeds the diffusion width $\Omega_p=k_p u_* \gg k_p\sqrt{D/\Gamma_m}$, the pumping field creates no inversion for particles with negative velocity $u=-u_*$, i.e., $\Delta N_{ml}(-u_*)$ can be ignored. Then the amplification of the opposite wave is absent. Thus, the frequency dependence of the standing-wave gain copies the shape of nonlinear correction $\delta\rho_m$ to the upper-level population. Consequently, the deviation from equilibrium occurs even at low output intensity domain, where saturation effects are absent. This feature distinguishes the effect from the Lamb dip [28]. The Lamb dip is a nonlinear effect and it requires saturation on the working transition. The saturation in our case makes the quantitative consideration more complicated, however, it does not change the main conclusion about the diffusional nature of the peak.

C. Raman gain

To derive the expression for spectral profile we take into account the saturation effects on the working transition ml, but restrict our consideration to the linear approximation with respect to the pumping intensity, i.e., ignore saturation on transition mn. The polarization at allowed transitions as a function of velocity u has the shape of narrow contours centered at $u=\Omega_p/k_p=\Omega/k$ for $\rho_+(u)$ and $\rho(u)$ or $u=-\Omega/k$ for $\rho_-(u)$. The width of each contour is determined by the dephasing $\delta u \sim t_D^{-1}/k \sim (D/k)^{1/3} \ll \sqrt{D/\Gamma_j}$. In accepted approximations, kinetic equation (3.2) gives the integrals for polarizations

$$2\ \mathrm{Re}(iG^*S_\pm)=\frac{2\pi|G|^2}{k}(\rho_m-\rho_l)|_{u=\pm u_*},$$

$$2\ \mathrm{Re}(iG_\mathrm{p}^*S)=\frac{2\pi|G_\mathrm{p}|^2}{k_p}(\rho_m^0-\rho_n^0)|_{u=u_*}, \qquad (3.3)$$

where

$$S_\pm=\int du\,\rho_\pm(u), \quad S=\int du\,\rho(u).$$

In Eq. (3.2) for populations, the narrow functions can be replaced by δ functions

$$\rho_\pm(u)=S_\pm\delta(u\mp u_*).$$

After this replacement the equations for populations take the following form:

$$\Gamma_l\rho_l=D\frac{d^2\rho_l}{du^2}+\mathcal{S}+A_{ml}(\rho_m-\rho_m^0)+\Gamma_l\rho_l^0,$$

$$\Gamma_m\rho_m=D\frac{d^2\rho_m}{du^2}-\mathcal{S}-\frac{2\pi|G_\mathrm{p}|^2}{k_p}\delta(u-u_*)[\rho_m^0(u_*)-\rho_n^0(u_*)]+\Gamma_m\rho_m^0, \qquad (3.4)$$

$$\mathcal{S}=\frac{2\pi|G|^2}{k}\{\delta(u-u_*)[\rho_m(u_*)-\rho_l(u_*)]+\delta(u+u_*)[\rho_m(-u_*)-\rho_l(-u_*)]\}.$$

In the Doppler limit $kv_T\to\infty$ the set is reduced to algebraic equations that can be solved analytically.

First, let us show how to solve set (3.4) without spontaneous decay ($A_{ml}=0$), then we treat the general case. We seek the population distributions as two exponential curves

$$\rho_j=\rho_j^0+A_j^+\exp\left(-\frac{|u-u_*|}{\sqrt{D/\Gamma_j}}\right)+A_j^-\exp\left(-\frac{|u+u_*|}{\sqrt{D/\Gamma_j}}\right). \qquad (3.5)$$

Substituting Eq. (3.5) into Eq. (3.4) we get the following equations for $A_j^{\pm}$:

$$2\sqrt{D\Gamma_l}A_l^{\pm}=\frac{2\pi|G|^2}{k}[\rho_m(\pm u_*)-\rho_l(\pm u_*)],$$

$$2\sqrt{D\Gamma_m}A_m^{+}=-\frac{2\pi|G|^2}{k}[\rho_m(u_*)-\rho_l(u_*)]-\frac{2\pi|G_p|^2}{k_p}[\rho_m^0(u_*)-\rho_n^0(u_*)],$$

$$2\sqrt{D\Gamma_m}A_m^{-}=-\frac{2\pi|G|^2}{k}[\rho_m(-u_*)-\rho_l(-u_*)].$$

Expressing the population difference at point $u=\pm u_*$ in terms of $A_j^{\pm}$ again, we obtain a linear set of equations for amplitudes $A_j^{\pm}$. Calculated amplitudes allow one to find the power generated from the unit volume at working frequency ω as a function of the pump detuning Ω_p using Eqs. (3.1) and (3.3):

$$\mathcal{P}(\Omega_p)=\frac{2\pi\hbar\omega|G|^2}{k}[\Delta N_{ml}(u_*)+\Delta N_{ml}(-u_*)]=\frac{2\sqrt{\pi}\hbar\omega|G|^2 f_T}{kv_T}\frac{2N_{ml}+PN_{nm}(1+e^{-z})}{1+p(1+q+e^{-z}+qe^{-z/q})},\tag{3.6}$$

where $f_T=\exp(-\Omega_p^2/k_p^2v_T^2)$ is the Doppler factor, $z=2|\Omega_p|/k_p\sqrt{D/\Gamma_m}$ is the detuning of the pumping field normalized to the diffusion width, $q=\sqrt{\Gamma_m/\Gamma_l}$ is the ratio of diffusion widths of levels l and m, $N_{ij}=N_i-N_j$ is the population difference, and $p=\pi|G|^2/\sqrt{Dk^2\Gamma_m}$ and $P=\pi|G_p|^2/\sqrt{Dk_p^2\Gamma_m}$ are the dimensionless Raman-laser and pump-wave intensity, respectively.

Expression (3.6) consists of two terms. The first one describes the linear absorption or amplification and is proportional to the unperturbed (equilibrium) population difference N_{ml} at the working transition. The second term is responsible for amplification induced by the optical pumping and proportional to the product PN_{mn} of the pump power and the population difference between starting and intermediate levels N_{nm}. In our experiments $N_n\gg N_m,N_l;PN_{nm}\gg N_{ml}$, therefore the second term, i.e., the optical pumping, prevails. The pumping induces the peak at $|\Omega_p|<0.5\sqrt{Dk_p^2/\Gamma_m}$. Its shape is described by a sharp exponential curve, a copy of the Bennett peak in the velocity distribution (3.5) at the upper level m. Its height significantly exceeds the linear amplification. In the case of weak saturation $p\ll 1$, the denominator (3.6) is independent of z. The contrast C of the peak can be defined as the amplification at its center $z=0$ divided by that at the wings $z\gg 1$. The contrast turns out to be $C=2$.

In the limit of strong saturation $p\gg 1$, we can ignore 1 in the denominator (3.6). At $q\gg 1$, i.e., for the long-lived lower level, the narrow peak in the gain contour induced by the pumping is also observable under strong saturation. Its profile is cusplike and given by the exponential curve and its width is determined by the diffusion at the upper level m again. Its contrast $C=2$ is the same, but its height is lowered by factor pq. In the opposite limit of short-lived lower level $q\ll 1$, as well as for equal relaxation constants $q=1$, the cusp in the gain disappears, since factors $(1+e^{-z})$ in the numerator and denominator cancel out. In the intermediate case $q>1$, the peak can combine with a wide dip. Its width is limited by diffusion at the lower level l; $\Delta\Omega=\sqrt{Dk_p^2/\Gamma_l}$. An analogous two-scale contour has been discussed concerning experiments on the Lamb dip in ionic spectra of a two-level system with different level lifetimes [20].

D. Self-consistent Raman lasing

To derive the expression for self-consistent generation power of the Raman laser, let us equate the gain of induced radiation to the losses in the cavity

$$\mathcal{P}(\Omega_p)=\frac{c|\mathcal{E}|^2}{8\pi}\frac{1-r}{L},$$

where r is the reflection coefficient of the coupling mirror, $1-r\simeq T$, and L is the length of active part of the medium. Neglecting absorption of the pump wave we get the intracavity intensity

$$p(z)=\frac{\mathcal{N}f_T+Pf_T(1+e^{-z})-\tau}{\tau(1+q+e^{-z}+qe^{-z/q})},\tag{3.7}$$

where

$$\mathcal{N}=2\frac{N_m-N_l}{N_n-N_m}$$

is the dimensionless population difference on the working transition, and

$$\tau=\frac{c|\mathcal{E}|^2}{8\pi}\frac{1-r}{L}\frac{kv_T}{2\hbar\omega\sqrt{\pi}|G|^2(N_n-N_m)}$$

is the dimensionless level of losses.

While we seek p, we assume the pump power P constant. For a real laser, the pumping field is inhomogeneous along the medium due to its absorption. To take the absorption into account we should average the calculated exponential dependence over the coordinate $P(x)=P\exp(-\alpha f_T x)$:

$$\langle P\rangle=\frac{1}{L}\int_0^L P(x)dx=P\frac{1-\exp(-\alpha f_T L)}{\alpha f_T L},$$

where P is the incident intensity of the pump field, α is the absorption coefficient at the line center. If we include also the spontaneous decay at the working transition, the method of calculation is almost identical. The final expression for the output power, including both effects of the spontaneous decay and inhomogeneous pumping field, has the following form

$$W_{\mathrm{AS}}=cp(z),$$

$$p(z)=\frac{\mathcal{N}/\tau f_T-1+\langle P\rangle f_T/\tau(1+e^{-z}-\mathcal{B})}{1+q+e^{-z}+qe^{-z/q}-\mathcal{B}}\geqslant 0, \quad (3.8)$$

where

$$\mathcal{B}=A\frac{q-1+qe^{-z/q}-e^{-z}}{q^2-1},$$

$A=A_{ml}/\Gamma_l$, $c=TS\sqrt{Dk^2/\Gamma_m}/A_{ml}$ is the dimensional scale factor, and S is the average cross section of the light beam. Equation (3.8) is the solution of the self-consistent problem on Raman lasing provided the amplification exceeds the losses. If the losses are greater [numerator (3.8) is negative], then $p(z)=0$ is the steady-state solution.

In a similar manner as Eq. (3.6), $p(z)$ could be split into two terms, that describe completely different phenomena. The first term, proportional to $\mathcal{N}f_T/\tau-1$, is responsible for conventional lasing on the working transition. The second term describes the Raman lasing due to the optical pumping and includes the parameters of all three levels. The first term has a frequency (z) dependence in the denominator only, which is caused by the saturation effect. When the gain is above the threshold $\mathcal{N}/\tau>1$, and pumping is negligible $\langle P\rangle\ll\mathcal{N}-\tau$, we obtain the Lamb dip in the spectral profile [28]. Its cusplike profile is determined by the Coulomb collisions [20].

In the opposite limiting case of strong optical pump $\langle P\rangle \gg|\mathcal{N}-\tau|$ z dependence enters in both the numerator and denominator of the second term. Generally, they lead to formation of a narrow peak with the diffusion width of the upper level and a wide dip with the diffusion width of the lower level. The qualitative behavior at $A\neq 0$ remains almost the same. Contrary to $A=0$, the factors involving z dependence do not cancel each other, even at $q\to 1$. Note that the generated power is proportional to the pump power P. This is a particular feature of the Raman laser in contrast to the two-level laser.

An additional contribution into the peak appears from the first term of Eq. (3.8) when the losses prevail at the working transition $\mathcal{N}<\tau$. This effect is analogous in some respects to saturated absorption peak [29], but can be observed only at presence of pumping $\langle P\rangle\gtrsim\tau-\mathcal{N}>0$. The generation is possible when the optical pump compensates the losses. This contribution is independent of P and allows subtracting it from the total line profile. Moreover, the second term in Eq. (3.8), proportional to P, starts to dominate already at relatively small excess above the generation threshold.

Thus, the peak in the spectral profile is formed due to diffusion in the velocity space, provided that the widths of resonant structures on levels m and l are different. This difference exists even for equal relaxation constants $\Gamma_m=\Gamma_l$ if spontaneous emission is taken into consideration.

IV. COMPARISON BETWEEN THEORY AND EXPERIMENT

Spectral profiles measured at different pump laser power are shown in Fig. 5. The experiment was performed within the scope of the theory. Three top curves 1, 2, and 3 were recorded at the same discharge pressure, while for the bottom curve 4 the pressure was higher. In the same picture, the theoretical curves calculated with formula (3.8) are also presented. Curves 1, 2, and 3 were fitted by parameter $q=\sqrt{\Gamma_m/\Gamma_l}$ and scale factor c. Parameters P/τ and $\mathcal{N}/\tau$ have been estimated from independent measurements. In the data processing, the following values are assumed: $\nu=2D/v_T^2=0.1\Gamma_m$, $\mathcal{N}/\tau=0.53$, $kv_T=3.2$ GHz, $\alpha L=1.5$, and $A=0.5q^2$ according to experimental conditions. The fitting was carried out using the central part of the curves ($|\Omega_p|<k_pv_T$), since the approximation underlying the theory is not valid at the wings.

As a result of the least-square fitting, the common value $q=1.3$ is obtained for curves 1, 2, and 3. This value corresponds to $\Gamma_m/\Gamma_l\simeq 1.7$ and agrees with the literature. As mentioned in Sec. II, the data on the lifetime of final level $4s'\,^2D_{5/2}$ by different authors [22,23] vary by a factor of 3. The present fitting makes it possible to measure the lifetime ratio more accurately. From known value $\Gamma_m^{-1}\simeq 6$ ns we obtain $\Gamma_l^{-1}\simeq 10$ ns with collisional deactivation included. For the bottom curve 4, the value $q=1.3$ was assumed and $\mathcal{N}/\tau$ became the fitting parameter. The result is $\mathcal{N}/\tau=5.6\times 10^{-3}$, which almost matches the threshold of linear absorption. The independent measurement in the ''high-Q'' cavity agrees well with this value.

Figure 5 confirms that the shape of spectral profile persists at increasing P. The width of the peak is governed by the velocity change on level m: $\delta_m=kv_T\sqrt{\nu/2\Gamma_m}=0.7$ GHz. We should take into account that the peak in the spectral profile is twice as narrow as the Bennett-type hole in the velocity distribution in frequency units. The tunability range depends on the excess of the amplification above the generation threshold. The excess is determined by both pumping P and linear gain $\mathcal{N}$ in agreement with Eq. (3.8). The absence of wings under higher pressure is a result of decreased linear gain $\mathcal{N}$ at the same pumping P. The same reason increases the fluctuations: points in series 4 are scattered, since the gain approaches the threshold. Figure 5 also indicates that the height of the peak is slightly above the theoretical prediction. Possible explanation is the saturation effect with respect to the pumping field ignored in the theory. At $|\Omega_p|>k_pv_T$ the contribution of the two-photon coherence effect grows and may lead to the observed deviations at the wings.

Absolute height of the peak (minus the pad) grows up linearly with pumping P. It points to the main role of the second term of formula (3.8) proportional to the pumping P and indicates that the effects like saturated absorption [29] are negligible under experimental conditions. Qualitative understanding of the main processes permits us to compare Fig. 4 with the theory, although the near-electrode plasma absorption is not known exactly. If we fit only the central peak, then the least-squares yield a reasonable parameter $q=1.2$, which agrees with the data extracted from Fig. 5. The theory does not describe the wings of the spectral profile, average absorption along the tube at the working transition and corresponding absolute value of $\mathcal{N}$ significantly changes with

the detuning in contrast to the basic assumptions of the theory.

V. CONCLUSIONS

We have shown that peculiarities of plasma as an active medium fundamentally modifies the spectral profile of the ion Raman laser with traveling pump wave and standing output wave. As distinct from the neutral gas, a comparatively broad peak is observed instead of a narrow two-photon dip. Its shape coincides with that of the collisionally broadened Bennett hole at the intermediate level. Its width is about 700 MHz, which exceeds the width of the forbidden transition by more than an order of magnitude.

The convenient theory of Raman lasing is often based on the assumption of output field being weak compared to the pumping power. It therefore ignores the saturation on the working transition. The generated wave in our experiment happened to be strong, so that its interpretation lies beyond the scope of the perturbation theory. We develop the alternative model describing the strong field on the working transition and weak pumping field. The second unusual feature of our theory is collisional dephasing of the forbidden transition polarization. Soft ion scattering in plasma turned out to be sufficient to destroy the coherence effects within the Doppler contour. The theory also provides the answer to the question on why the slope of the frequency characteristics is determined by the ratio of wavelengths even off the Doppler contour. The coherence effect breaks the symmetry between two counterpropagating waves. Because of the nonlinear mode competition, only the wave parallel to the pumping one is generated.

The proposed model describes well the experimental spectral profiles $W_{\mathrm{AS}}(\Omega_p)$ for various pump powers and discharge pressures. The sharp peak with contrast 1.5–2 against the smooth background was observed within the broad domain of parameters. Under some conditions the isolated peak without a pad was registered, or the peak inside a smooth dip. Each case agrees qualitatively with the theory.

The shape of spectral profile is very sensitive to the ratio of working level lifetimes Γ_m/Γ_l and the effective transport frequency ν. That permits one to utilize the effect for the determination of one lifetime provided the other is known. Such an estimation has been done in the present paper for an Ar II metastable levels in plasma. If both lifetimes are measured independently, then the collision frequency can be extracted from the peak shape. Thus the effect may also be helpful for plasma diagnostics.

ACKNOWLEDGMENTS

We are grateful to A. M. Shalagin and S. G. Rautian for fruitful discussions, and M. A. Rybakov for technical assistance. This work is partially supported by RFBR Grant Nos. 00-02-17973 and 00-15-96808, and by Russian Ministry of Science and Technology, program ''Physics of Quantum and Wave Processes.'' M.G.S. acknowledges the support by INTAS within the program of the International Center for Fundamental Physics in Moscow No. 96-0457. Tunable cw dye laser for the experiments is courteously granted by Laser Center ''Inversion'' (Novosibirsk).

[1] R. Corbalán, J. Cortit, and F. Prati, Phys. Rev. A **53**, 481 (1996).
[2] A.J. Merriam and A.V. Sokolov, Phys. Rev. A **56**, 967 (1997).
[3] V.V. Kozlov, P.G. Polynkin, and M.O. Scully, Phys. Rev. A **59**, 3060 (1999).
[4] A. Eschmann and R.J. Ballagh, Phys. Rev. A **60**, 559 (1999).
[5] C.L. Bentley, Jr., J. Liu, and Y. Liao, Phys. Rev. A **61**, 023811 (2000).
[6] A.A. Apolonsky *et al.*, Phys. Rev. A **61**, 033408 (2000).
[7] I.M. Beterov and V.P. Chebotaev, Prog. Quantum Electron. **3**, 1 (1974).
[8] B. Wellegehausen, IEEE J. Quantum Electron. **15**, 1108 (1979).
[9] J.C. White, Top. Appl. Phys. **59**, 115 (1989).
[10] K.S.E. Eikema, J. Waltz, and T.W. Hänsch, Phys. Rev. Lett. **83**, 3828 (1999).
[11] U. Hinze, L. Meyer, E. Chichkov, B. Tiemann, and B. Wellegehausen, Opt. Commun. **166**, 127 (1999).
[12] M. Jain *et al.*, Phys. Rev. Lett. **77**, 4326 (1996).
[13] S.F. Yelin, M.D. Lukin, M.O. Scully, and P. Mandel, Phys. Rev. A **57**, 3858 (1998).
[14] A. Feitisch, D. Schnier, T. Müller, and B. Wellegehausen, IEEE J. Quantum Electron. **24**, 507 (1988).
[15] A.A. Apolonsky *et al.*, Phys. Rev. A **55**, 661 (1997).
[16] K. Rittner, A. Höpe, T. Müller-Wirts, and B. Wellegehausen, IEEE J. Quantum Electron. **28**, 342 (1992).
[17] V.S. Letokhov and V.P. Chebotaev, *Nonlinear Laser Spectroscopy* (Springer-Verlag, Heidelberg, 1977).
[18] S.G. Rautian and A.M. Shalagin, *Kinetic Problems of Non-Linear Spectroscopy* (Elsevier, Amsterdam, 1991).
[19] E.V. Baklanov, I.M. Beterov, B.Y. Dubetsky, and V.P. Chebotaev, Pis'ma Zh. Éksp. Teor. Fiz. **22**, 289 (1975) [JETP Lett. **22**, 134 (1975)].
[20] S.A. Babin and D.A. Shapiro, Phys. Rep. **241**, 119 (1994).
[21] S.A. Babin, S.I. Kablukov, and S.M. Kobtsev, Opt. Spectrosk. **84**, 915 (1998) [Opt. Spectrosc. **84**, 828 ((1998)].
[22] B.F.J. Luyken, Physica **60**, 432 (1972).
[23] A. Hibbert and J.E. Hansen, J. Phys. B **27**, 3325 (1994).
[24] C.C. Davis and T.A. King, Adv. Quant. Electr. **3**, 169 (1975).
[25] M.H. Dunn and J.N. Ross, Prog. Quantum Electron. **4**, 233 (1976).
[26] S.A. Babin and A.E. Kuklin, SPIE Proc. **1397**, 589 (1991).
[27] G.I. Smirnov and D.A. Shapiro, Zh. Éksp. Teor. Fiz. **76**, 2084 (1979) [Sov. Phys. JETP **49** (6), 1054 (1979)].
[28] W.E. Lamb, Phys. Rev. **134**, 1429 (1964).
[29] V.N. Lisitsyn and V.P. Chebotaev, Zh. Éksp. Teor. Fiz. **54**, 419 (1968) [Sov. Phys. JETP **27**, 227 (1968)].